Earth Planet. Sci. Lett. 633 (2024) 118638

Contents lists available at ScienceDirect

Earth and Planetary Science Letters

journal homepage: www.elsevier.com/locate/epsl

Revisiting the discrimination and distribution of S-type granites from zircon trace element composition

Nick M W Roberts [a,*], Chris Yakymchuk [b], Christopher J Spencer [c], C. Brenhin Keller [d], Simon R Tapster [a]

[a] Geochronology and Tracers Facility, British Geological Survey, Nottingham, NG12 5GG, England
[b] Department of Earth and Environmental Sciences, University of Waterloo, Waterloo, Ontario N2L 3G1, Canada
[c] Department of Geological Sciences and Geological Engineering, Queen's University, Kingston, Ontario, Canada
[d] Department of Earth Sciences, Dartmouth College, Hanover NH, USA

ARTICLE INFO

Keywords:
Zircon
Trace elements
S-type granite
Redox
Early earth
Supercontinents

ABSTRACT

Trace element compositions of zircon can be used to estimate the chemistry of their host magmas; as such they provide a useful tool in zircon provenance, and in the assessment of changing magma chemistries in time and space. Granites derived from the melting of sedimentary protoliths (S-types) have previously been discriminated by their P contents and P vs. REE+Y correlations, largely based on data from the Lachlan Fold Belt. Using a range of magmatic suites from different locations, we show that this discrimination commonly fails to discriminate S-type granite from others. We propose an alternative discrimination tool, based on a plot of Ce/U vs. Th/U, which makes use of low LREE/U and Th/U in metapelite-derived melts. Through coupled thermodynamic and accessory mineral saturation modelling, we demonstrate that these low ratios can be explained by monazite co-crystallisation. We demonstrate that Himalayan S-types, which are inferred to have formed from partial melting of metapelite, and thus can be classified as pure S-types, exhibit the lowest Ce/U and Th/U ratios, and overlap those of metapelitic zircon. Granites formed in oceanic arcs (I-types) and mantle-derived suites both have the highest Ce/U and Th/U ratios. Other S-types, such as those known to have mixed sedimentary and igneous protoliths, which we term Hybrid S-types, form a field overlapping pure I- and S-types. We use Ce/U versus Th/U to demonstrate the dominant I-type origin to early Earth (>3.6 Ga) zircon, and using a large detrital zircon database we assess the proportion of S-type zircon through Earth history. In contrast to previous findings, we find that the supercontinent Rodinia had a normal abundance of S-type zircon, as with other supercontinents, and that instead the period 1.7–1.2 Ga exhibits a marked low in S-type zircon, corresponding to fewer continental collisions.

1. Introduction

Although the value of granite classification schemes is oft questioned, discrimination of granite-forming processes is useful for understanding the long-term formation and differentiation of the continental crust. The I- and S-type granite divide was formulated based on granites exposed in the Lachlan Fold Belt of SE Australia (Chappell and White, 1974) and is most commonly inferred to represent igneous and sedimentary protoliths, respectively. An important caveat is that some I-type granites may be derived from immature clastic sedimentary rocks (e.g. Clements et al., 2011), whereas S-type granites are almost exclusively generated from aluminous sedimentary rocks. S-type granites can be discriminated based on mineralogy, chemistry or source, but no formal classification scheme has been adopted. For geochemical classification, K/Na, aluminium saturation (either as Aluminium Saturation Index - ASI or MALI – Modified Alkali-Lime Index) and P contents are commonly used parameters (Chappell and White, 1992; Clemens et al., 2011; Bucholz et al., 2018). Mineralogically, S-type granites are associated with the presence of one or more aluminous phases, such as garnet, cordierite, and muscovite; consequently, two-mica granites are often classified as S-types. High aluminium content is related to a source that has been weathered surficially, such that clay is incorporated, which has Al enriched relative to K and Na (Chappell and White, 1992). Therefore, it is aluminium, through the incorporation of clay, providing the

* Corresponding author.
E-mail address: nirob@bgs.ac.uk (N.M.W. Roberts).

https://doi.org/10.1016/j.epsl.2024.118638
Received 30 November 2023; Received in revised form 2 February 2024; Accepted 26 February 2024
Available online 12 March 2024

necessary elements for aluminous mineral stability, that forms the basis of the generalized S-type scheme.

The use of trace elements in zircon to discriminate magmatic suites has been slow to develop, with early studies showing significant overlap in trace element space (Hoskin and Ireland, 2000; Belousova et al., 2002), and the most commonly used discriminants being for tectonic setting (e.g. Grimes et al., 2007, 2015). Over recent years, several schemes have been presented for the discrimination of S-types. Burnham and Berry (2017) demonstrated that I- and S-type granites from the Lachlan Fold Belt were different in both their P contents and P vs. REE+Y correlations. Since then, P content has commonly been used to discriminate S-type-derived zircon within detrital zircon datasets (Tang et al., 2021; Brudner et al., 2022; Liu et al., 2022a, 2022b; Chen, 2023). Furthermore, Zhu et al. (2020) used the P vs REE+Y classification to determine the abundance of S-type granites through time, which showed a heterogeneous distribution correlative to supercontinent cycles. However, recent work demonstrated that P content in strongly peraluminous granites (SPGs), which are broadly synonymous with S-types, has varied through time (Bucholz, 2022), and therefore, that Precambrian (SPGs) do not fit the Lachlan-based discrimination (Bucholz et al., 2022). As a consequence, questions remain over the robustness of P content as a zircon discrimination tool. Other attempts at S-type classification have focused on: 1) depletion of Nb, Ta and Ce relative to P (Sawaki et al., 2022a, 2022b); 2) their HREE and Th/U ratios (Breiter et al., 2014); or 3) depletion of Nb (and Th) relative to Pb (Wang et al., 2012). More recently, machine learning methods that integrate multiple variables have been used to classify S-types (Zhong et al., 2023a, 2023b), like with many previous studies, these indicate low Eu/Eu*, Ce/Ce* and Th/U ratios in zircon as characteristics of S-type granites (e.g. Wang et al., 2012; Sawaki et al., 2022b; Tang et al., 2021).

However, several issues limit the applicability of these studies throughout space and time, particularly that either: (1) the scheme was based on a limited number of granite suites, and thus may not be representative (Breiter et al., 2014; Burham and Berry, 2017; Sawaki et al., 2022a, 2022b); or (2), was based on classification of granite suites with no definition provided (Zhong et al., 2023a, 2023b). As with studies such as Tang et al. (2021), where the classification relied on that of the primary literature, we assume that the latter may mix mineralogical, geochemical and source-based inference for granite classification; this approach limits our ability to test the veracity of zircon-based classification against whole-rock geochemical classification.

Here, we re-examine the zircon trace element discrimination of I- vs. S-type granites. We attempt to address previous issues by examining a greater number of sample suites, and by using clear means of classification, whether those be based on mineralogy, geochemistry and/or known affinity to source materials. We demonstrate that P content and P vs. REE+Y correlations are not robust discriminators of magma composition, and that S-type and I-type granites have significant overlap in their trace element signatures. We present a discrimination tool, log (Ce/U) vs. log(Th/U), which makes use of the Th and Ce (LREE) depletion common to anatectic melt and associated zircon in compositions where monazite is stable. These ratios distinguish pure metapelite-derived melts, which can be considered end-member S-type granites, from I-type 'mantle-derived' melts. Finally, using a database of detrital zircon trace element compositions, we readdress the abundance of S-type granites through time, as well as the much-debated origin of early Earth (>3.6 Ga) zircon.

2. Data

We compiled ~6500 igneous and ~3000 metamorphic zircon trace element compositions from the literature. In addition, we added ~700 zircon compositions from our own analyses. The full datasets, data sources, filtering criteria, and methods for new data acquisition, are compiled in the supplementary files. We have classified our database into a number of suites, using a variety of means, with the aim of objectively addressing zircon-based discrimination. Lachlan Fold Belt granites use the I- and S-type samples according to the original source, and as used by Burnham and Berry (2017) and Zhu et al. (2020). From the literature we manually identified a number of magnesian (I-type) and ferroan (A-type) suites categorized by their whole-rock geochemistry and Fe-index (Frost et al., 2001). S-type suites were identified by mineralogical criteria (presence of muscovite ± garnet ± cordierite), with the addition of having pelitic source materials identified in the literature. We also compile data from: 1) 'mantle-derived' suites (data from Mid-Ocean Ridges and Iceland); 2) 'Oceanic Arc' suites from a range of well-known modern active margins; and 3) a range of SPG (Strongly Peraluminous Granite) suites, based solely on a whole-rock ASI (Aluminium Saturation Index) of >1.2. The latter overlap the compilation of S-type suites, but are strictly based on geochemistry and may thus not meet the same mineralogical and source-based criteria, and will likely also include highly differentiated I-type granites. Finally, we compiled metamorphic zircon data from the literature, which comprise both sub-solidus and supra-solidus zircon compositions grown within metamorphic rocks of variable lithologies under a wide range of pressures and temperatures.

3. S-type discrimination

3.1. Discrimination based on phosphorus content

Burnham and Berry (2017) used granites from the Lachlan Fold Belt in SE Australia to demonstrate that I- and S-type granite types could be discriminated by their zircon trace element signatures. I-types had lower P contents and no correlation with rare earth elements (REE), and S-types had much higher P contents on average, as well as exhibiting a broad 1:1 trend with REE contents (when plotted as molar P versus molar REE+Y; Fig. 1a). They argued that a cut-off at >750 ppm (equivalent to molar P = 30) would discriminate most S-types. Zhu et al. (2020) supplemented data to this from another suite of S-type granites exposed in the Bohemian Massif that also exhibited the same behaviour as the LFB S-types. However, Bucholz et al. (2022) recently showed that Precambrian SPGs do not conform to the LFB-based trends. We demonstrate this latter observation in Fig. 1b, where all Precambrian SPGs fall below the 750 ppm cut-off.

Using both new and existing zircon trace elements from various magmatic suites, we take the observations of Bucholz et al. (2022) further. In Fig. 1b, we plot SPGs (whole-rock ASI >1.2) of the Phanerozoic versus those Precambrian in age. Although not completely synonymous with S-types, the SPGs show a greater proportion of zircon with 'normal' P contents compared to those of the Lachlan Fold Belt. In Fig. 1c, we present data from a selection of granitoid suites that have clear S-type affinity based on their mineralogy and geochemistry (i.e. muscovite-bearing and peraluminous). As with Fig. 1b, P contents of many S-type-derived zircon are well below the 750 ppm cut-off of Burnham and Berry (2017). A second important observation is that S-type-derived zircon can exhibit correlations between P and REE that are not necessarily 1:1.

In Fig. 1d and e, we show trends exhibited by a range of geochemically defined ferroan and magnesian suites, i.e. broadly equivalent to A- and I-types. Both of these have P contents similar to the LFB I-types; however, another critical observation is that these suites can also exhibit strong P vs. REE correlations, but in variable ratios of enrichment. Finally, in Fig. 1e we plot suites from Iceland and Mid Ocean Ridge sites (MOR), both of which are assumed to have mantle-derived affinity. Intriguingly, although derived from fractionation and/or partial melting of mantle-derived mafic rocks, the P contents of these are elevated above many I- and A-types.

Our data compilation demonstrates that P and REE contents across a range of a magmatic suites exhibit much greater variability in enrichment and trends than those used previously to determine an I- vs S-type classification (Burnham and Berry; 2017; Zhu et al., 2020). Therefore,

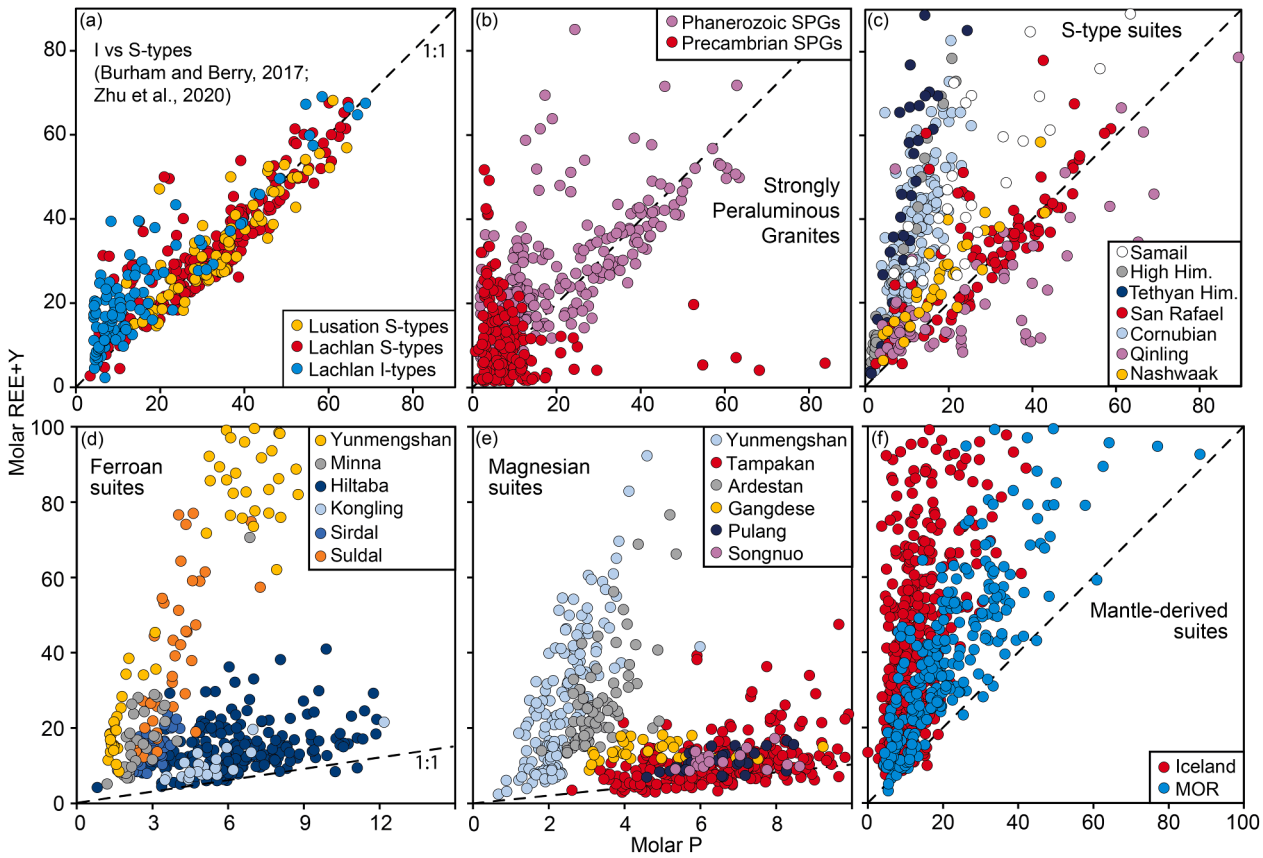

Fig. 1. Molar P vs. Molar REE+Y in zircon for various magmatic suites. (a) I- and S-types from the Lachlan Fold Belt and S-types from the Lusation Granodiorite Complex; (b) Comparison of Precambrian vs. Phanerozoic Strongly Peraluminous Granites (SPGs) defined by ASI > 1.2 (c) S-type suites defined by mineralogy (i.e. muscovite-bearing) and peraluminous geochemistry; (d) Ferroan suites defined by their geochemistry (Fe-index of Frost et al., 2001); (e) Magnesian suites defined by their geochemistry (Fe-index); (f) Mantle-derived suites from Iceland and Mid Ocean Ridge (MOR) sites.

although many S-types exhibit P contents much higher than the range of I- and A-types studied, P content alone cannot successfully discriminate granite type. Variable ratios of P enrichment relative to REEs and Y indicate the existence of REE substitution mechanisms other than xenotime substitution, as postulated for S-type granites (Burnham and Berry, 2017). Sawaki et al. (2022a, 2022b) previously discussed the variable behaviour of apatite and xenotime co-crystallisation on zircon REE incorporation, arguing that magma chemistry dictates the saturation of apatite and xenotime relative to zircon, which in turn leads to variable REE substitution mechanisms.

3.2. Th-Ce-U based discrimination

True S-type granites have sedimentary protoliths, thus, we sought to find a trace element discriminator that takes advantage of this feature. Metamorphic zircon, i.e. those grown from metamorphic processes such as solid-state reactions, dissolution-reprecipitation and peritectic reactions, have long been known to commonly exhibit depleted LREE and lower Th/U contents when compared to magmatic (or igneous) zircon (Rubatto, 2002; Hoskin and Schaltegger, 2003; Martin et al., 2008). The processes leading to this behaviour likely reflect multiple factors, including the presence of REE-bearing minerals and/or those with relatively high Th/U ratios such as monazite, titanite, allanite (for Light to MREE depletion), and changing lattice size and hence trace elemental partitioning (Chen and Zheng, 2017; Rubatto, 2017). Wooden et al. (2006) suggested a plot of Th vs. U/Ce can be used to discriminate magmatic from metamorphic zircon, and this has since been utilized by various authors (Castiñeiras et al., 2010, 2011; Marsh and Stockli, 2015). To assess the veracity of this plot for I- and S-type discrimination, we have taken the data from Fig. 1 and recast as Th vs U/Ce (Fig. 2a–F). We have redrawn a dividing line between magmatic and metamorphic line so that it falls between pure mantle-derived zircon (i.e. Iceland and Mid-Ocean Ridge) and those of metapelites (Fig. 2f). The result is that Lachlan Fold Belt I- and S-types fall below and above this line, respectively (Fig. 2a). Furthermore, the ferroan and magnesian suites fall generally within the magmatic field, except for the Gangdese suite which falls just above the line. The S-type suites generally either straddle this boundary (Qinling and Nashwaak), or fall above the line; an exception to this is the Samail mantle-hosted granitoids that mostly fall below the line. The compilations of SPGs overlap the space defined by both I- and S-types. Although there are some exceptions (i.e. Samail suite), which we will further discuss later on, U/Ce seems to reasonably discriminate I-types that overlap mantle-derived magmas with presumably no sedimentary contribution, and S-types that overlap the field of metapelitic zircon.

Because metapelitic and anatectic zircon have lower Th/U ratios as well as higher U/Ce ratios, we have recast this figure as log10(Th/U) vs log10(Ce/U) (Fig. 3a–i). Our reasoning is that this plot takes advantage of coupled depletion in Th and LREE compared to U for metapelitic rocks compared to magmatic rocks (Fig. 3f). Using log10(Ce/U) = −2 (equivalent to Ce/U = 0.01) and log10(Th/U) = −1 (equivalent to Th/U = 0.1) as dividing lines, metapelitic zircon generally fall within the bottom left quadrant, and mantle-derived zircon fall within the top right quadrant. We note the presence of some metapelitic zircon overlapping with magmatic ratios, and highlight that these are from high temperature rocks. The broad division in Ce/U ratios reasonably divides I- and S-type granites of the Lachlan Fold Belt (Fig. 3a). The equivalent patterns to those in Fig. 2 are also represented, with ferroan and magnesian suites

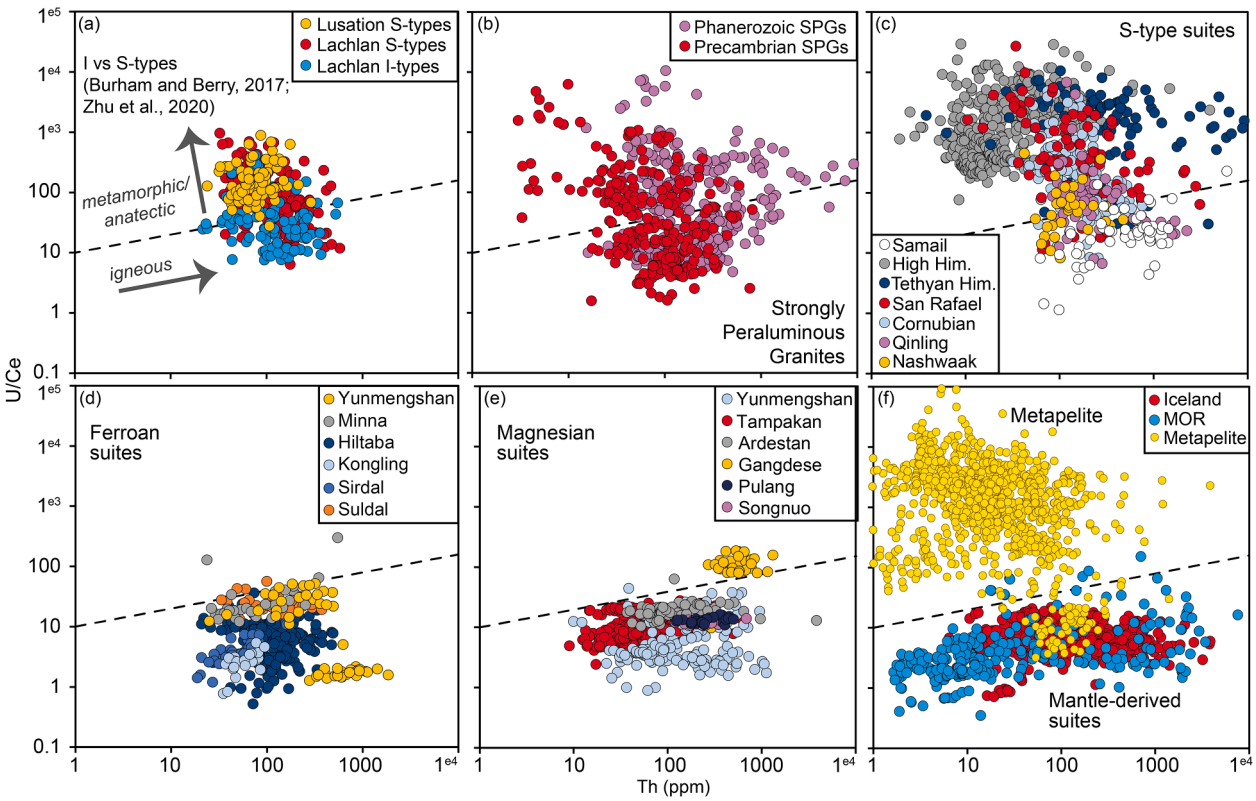

Fig. 2. (a–f) The same samples as Fig. 1 plotted as zircon Th (ppm) vs. U (ppm)/Ce (ppm). (c) contains additional data from the Tethyan Himalaya; (f) contains additional data from a compilation of metapelitic zircon. Him. = Himalaya; SPG = Strongly Peraluminous Granite; MOR = Mid-Ocean Ridge.

falling into the top-right quadrant (Figs. 3d-e), and S-type granites overlapping this field but trending to the bottom left (3b-c). In addition, we plot a compilation of metamorphic zircon compositions from a wide range of protoliths in Fig. 3 g; the implication of this specific plot is that magmatic zircon, neither I- or S-types, can be discriminated completely from metamorphic zircon - an observation already known for Th/U ratios (Yakymchuk et al., 2018). Overall the Ce/U vs. Th/U plot seems to successfully describe variable Th, Ce and U behaviour in granitic zircon. I-types, such as those found in oceanic arcs, overlap the presumably sediment-free mantle-derived field (Fig. 3h), whereas S-type granites from the Himalaya that can be considered pure S-type melts (Hopkinson et al., 2017) overlap the metapelite field.

An interesting observation from Fig. 3 is that the Himalayan suites are the only S-types represented in our compilation that completely overlap the metapelite field, whereas other S-types have greater overlap with the I-type field. To understand this, we have to consider the cause of this trace element behaviour. Unlike an isotopic signature, e.g. $\delta^{18}O$, the trace element ratios do not represent proportions of source materials. At equilibrium, they are dictated by partition coefficients, the melt composition, and the availability of trace elements. Theoretical modelling has shown that changes in zircon composition can be dominated by co-crystallisation or presence of other mineral phases, for example, monazite crystallisation depletes the melt in Th, leading to low Th/U in zircon grown contemporaneously (Yakymchuk et al., 2018). We use this modelling approach to demonstrate the role of monazite crystallisation in metapelite-derived melts upon the Ce/U ratios.

In Fig. 4, we show the results of an equilibrium model for melting of a metapelite and the evolving composition of zircon that is in equilibrium with melt and residue as a function of pressure and temperature. The proportion of anatectic melt in the system increases with temperature (Fig. 4a) whereas the amounts of zircon and monazite decrease. At temperatures just above the solidus, concentrations of all trace elements (Ce, U and Th) in modelled zircon are high (Figs. 4d–F); this reflects the very small melt fraction (<5 wt %) in the system at these conditions and the relative incompatibility of these elements in the residual mineral assemblage. These melt fractions are generally considered too low to reach melt connectivity and, therefore, the elevated concentrations of Th, U and Ce in zircon are not expected to be realized in S-type granites. Modelled concentrations of U in zircon decrease with increasing temperature (Fig. 4e) and this reflects the coupled incompatibility of U in the residual mineral assemblage and the increasing melt fraction that dilutes the melt in U (and the resultant equilibrium U concentrations in zircon). Thorium and cerium concentrations in zircon decrease with temperature up to ~800 °C—this reflects a similar dilution effect as for U—followed by an increase up to the conditions of complete monazite consumption (Figs. 4d, 4f). This increase in Ce and Th in zircon between ~800–850 °C up to a maximum at the conditions of monazite exhaustion reflects the very low mode of monazite at this point. After monazite exhaustion, the concentrations of Ce and Th decrease up temperature due to dilution because of increasing melt fraction. Zircon is expected to be completely consumed by ~850–900 °C in the model. Zircon Ce/U and Th/U ratios increase with temperature (Fig. 4 g, h). These increases are mostly controlled by the decrease of U up temperature. However, these increasing values also track the decreasing amount of monazite—a key mineral repository of Ce and Th—up temperature (Fig. 4c).

Although there are clear caveats and limitations to this modelling – equilibrium, distribution coefficients, starting compositions etc., the results show a clear link between LREE depletion in zircon and monazite abundance. Based on this, we argue that pure metapelite-derived S-type granites will overlap the field of metapelitic zircon; such anatectic granites can be considered an extension of crustal metamorphism, but are clearly an igneous product.

Why don't all S-types overlap the field of metapelitic zircon? This is likely due to two processes. First, at high temperatures, monazite may not be stable during partial melting (e.g. >800–850 °C in Fig. 4c), and thus zircon grown under these conditions will not exhibit low Th/U and

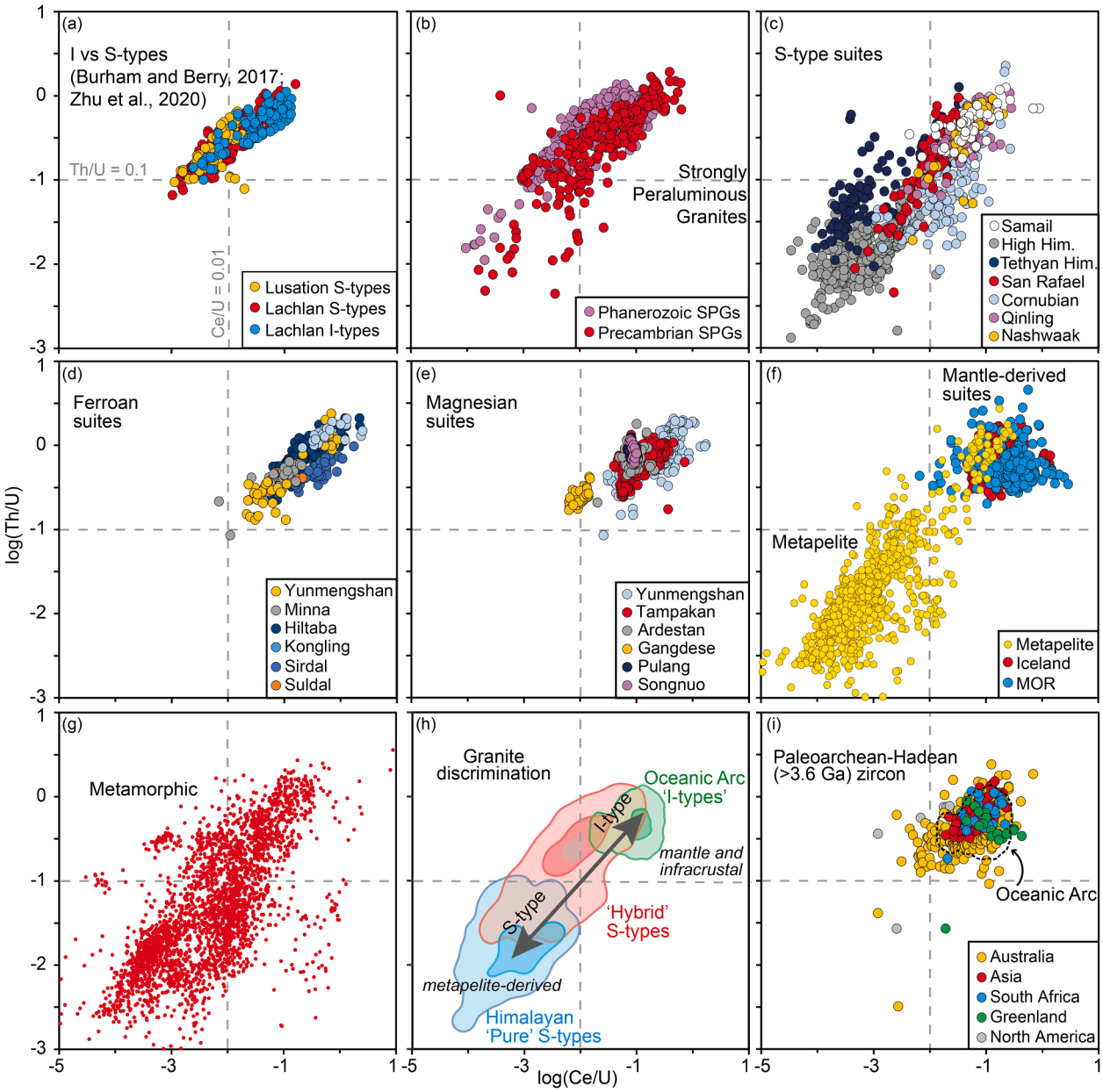

Fig. 3. (a-f) The same samples as in Fig. 2, plotted as log(Th/U) vs. log(Ce/U) (base 10). (g) Compilation of metamorphic zircon data; (h) Compilation of 'I-type' zircon from Oceanic Arcs, compared with those from the S-types in 3c (excluding the Himalaya), which we define as Hybrid S-types, compared with the Himalayan S-types which we interpret as Pure S-types. Data plotted as 2D kernel density estimates showing at 95 % and 50 %; (i) Compilation of igneous and detrital zircon data >3.6 Ga in age, colour-coded by continent, compared with 95 % density estimate of Oceanic Arc zircon compositions. Dividing lines are shown in all plots at Ce/U = 0.01 and Th/U = 0.1.

Ce/U ratios. Second, many S-types are hybrid granites, formed through interaction between sediment-derived melts with melting of juvenile mantle-derived crust, or melting of pre-existing meta-igneous crust (e.g. Keay et al., 1997; Healy et al., 2004; Harlaux et al., 2021). As such, the role of monazite crystallisation on Ce and Th depletion in the melt will be dampened, and/or, monazite stability will be decreased due to unfavourable melt chemistry. Those granites hypothesized to have formed from mixed parent magmas via geochemical and isotopic studies, such as the Lachlan Fold Belt (Healy et al., 2004), Cornubian batholith (Stimac et al., 1995) and San Rafael Intrusive Complex (Harlaux et al., 2021), overlap the fields of pure S-types and pure I-types. The Samail mantle-derived granites overlap the I-type field, providing a possible exception to our proposed Ce/U based S-type discrimination. These granitoids have variable compositions (Angelo et al., 2023), but are deemed to be formed via sediment (pelite) derived melts interacting with basaltic melts within the mantle wedge (Rollinson, 2015; Angelo et al., 2023), with melts forming at high temperatures. Although they have a strong sedimentary contribution (Spencer et al., 2017), there is no record of monazite as an accessory phase, as such they form a rather anomalous S-type end-member.

We argue that a plot of Ce/U vs Th/U can be used as a broad granite classification tool (Fig. 3h). The usual caveats regarding the use of discrimination plots apply, and the overlap with metamorphic zircon is a distinct hindrance when trying to classify the source of unknown zircon, such as those in the detrital record. However, this plot can be used in tandem with other geochemical data to characterize the petrogenesis of felsic igneous rocks.

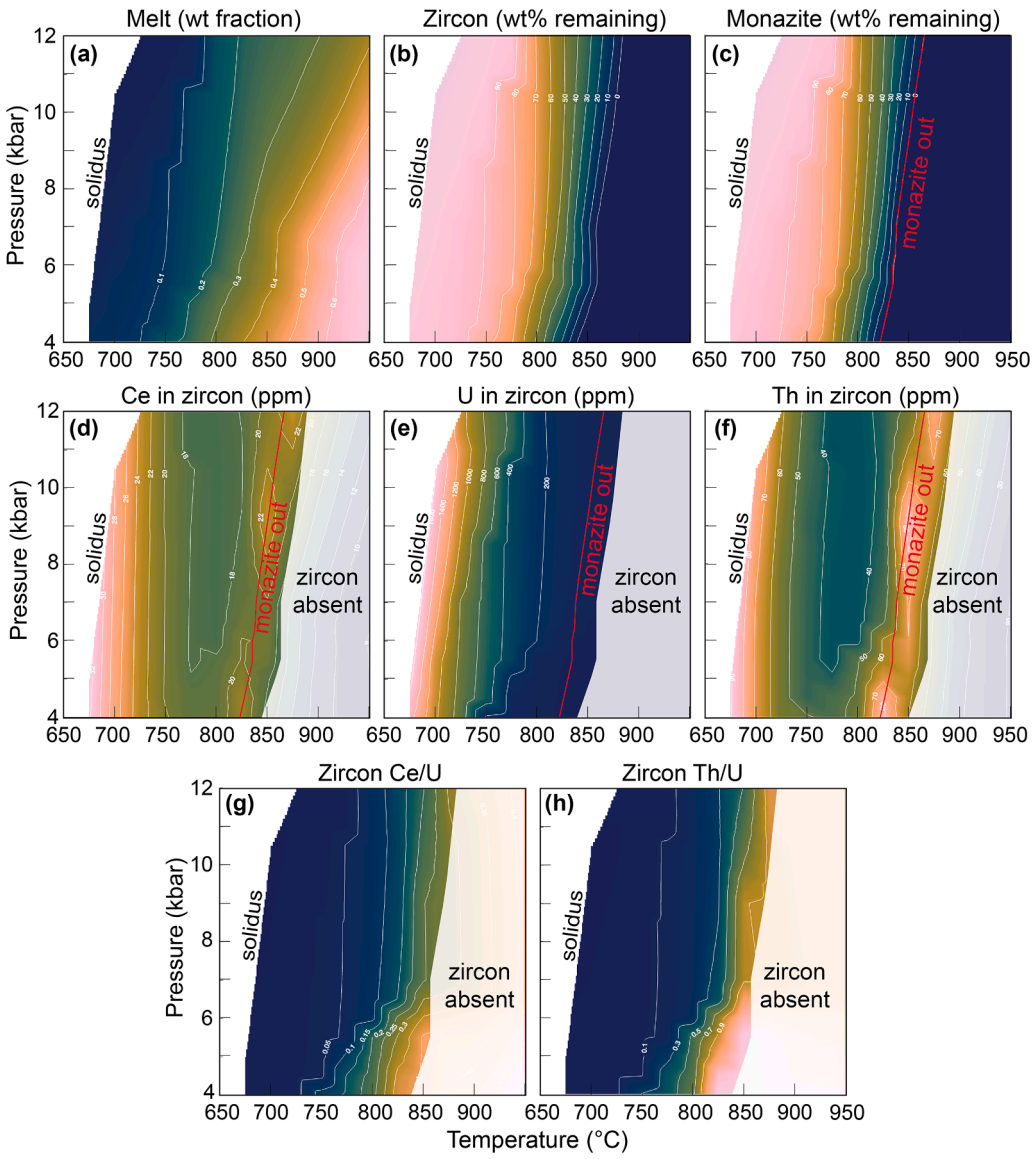

Fig. 4. Equilibrium modelling of high-temperature metamorphism and partial melting of a metapelite and the evolving equilibrium zircon compositions. (a) Weight fraction of anatectic melt in the system. Amounts of zircon (b) and monazite (c) are relative to the amount at the solidus. The monazite-out line is the 0 % remaining contour from (c). (d)-(f) Trace element compositions of equilibrated zircon. (g) and (h) show trace element ratios in equilibrated zircon. For (d) through (h), the zircon-absent fields represent pressure and temperature conditions above modelled terminal zircon stability in (b). Complete phase diagrams for the major mineral assemblages in this metapelite composition are found in Yakymchuk et al. (2023). Modelling methods are presented in the Supplementary Materials.

4. Implications for reduced nature of sedimentary melts and oxybarometry

S-type granites are thought to be more reduced than I-types (Chappell and White, 1992; Foden et al., 2015). It is therefore interesting that our S-type discriminant (Ce/U) is hypothesized to represent redox conditions of the host magma during zircon crystallisation (Loucks et al., 2020). This reflects the contrasting behaviour of Ce and U, with increasing and decreasing zircon/melt partition coefficients with increasing fO_2, respectively (Burnham and Berry, 2012; Loucks et al., 2018). Using U/Ti as a proxy for differentiation, the combined contents of Ce, U and Ti have been converted to ΔFMQ by Loucks et al. (2020), based on an empirical relationship. This relationship is mostly based on I-type magmas, but one S-type also aligns within the trend displayed by I-types; the authors note however, that the relationship remains untested for peralkaline or peraluminous systems. The fact that all S-type granites we present trend to lower Ce/U relative to I-types, suggests that S-types are indeed reduced (see Fig. 5). However, we relate low Ce/U ratios in part to depletion of LREE via monazite co-crystallisation; the significance of this is that low Ce/U presumably does not entirely relate to fO_2-dependant partitioning. To further demonstrate this, using other LREEs rather than Ce leads to similar behaviour in terms of LREE/U depletion in metapelites and S-type granites (see Fig. S1). As such, we suggest that the Ce-U-Ti based fO_2 proxy should be investigated for a greater range of magma compositions. Another corollary of the data we present, is that metamorphic zircon, especially those with a metapelitic protolith, also have low Ce/U and thus indicate apparent low ΔFMQ values, i.e. reducing conditions. Redox during metamorphism and partial melting are not well constrained, and thus whether low Ce/U (and LREE/U) in metamorphic zircon solely reflects co-crystallisation of LREE-bearing phases, or can be linked to reducing conditions, also provides an avenue for investigation.

5. The source of early earth zircon

Zircon provides the oldest record of the Earth's continental crust, and

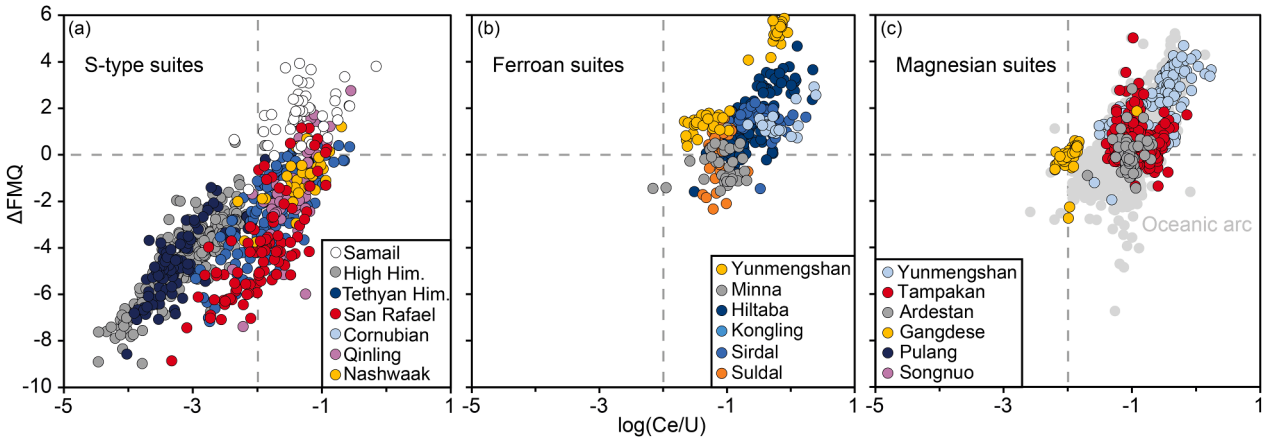

Fig. 5. (a-c) Sample data correlates to those of Figs. 2c-e and 3f, plotted as log(Ce/U) vs. ΔFMQ, where ΔFMQ is calculated using abundances of Ce, U and Ti in zircon following Loucks et al. (2020).

as such, the origin of Hadean to Paleoarchean zircon are much debated (see Harrison, 2020; Roberts and Spencer, 2015). A range of isotope, elemental and mineral inclusion data have been used to argue for contrasting tectono-magmatic settings, with key arguments centred on the existence or absence of subduction, water and felsic continental crust on Early Earth (e.g. Mojzsis et al., 2001; Harrison, 2009; Carley et al., 2014; Reimink et al., 2020; Drabon et al., 2022). Most recently, hypotheses for Hadean zircon have comprised formation in residual granitic melts (Laurent et al., 2022) and within shallow melting of hydrated peridotite (Borisova et al., 2022). Burnham and Berry (2017) used P vs. REE+Y to demonstrate that Jack Hills zircon, the dominant source of global Hadean zircon, exhibit I-type chemistry. However, Bucholz et al. (2022) questioned the validity of this argument after demonstrating that Archean S-type zircon cannot be distinguished by their P content. Most recently, Zhong et al. (2023a) used machine learning to classify trace element compositions of I-type, S-type and TTG compositions, and found that Jack Hills zircon comprised a large proportion of both I-and S-type derivation. Their model diverged from previous classifications in that TTGs were separated from I-types, even though TTGs can be classified as I-types if a simple protolith definition is used (I-type = igneous protolith; S-type = sedimentary protolith). Although the machine learning algorithm used many different trace element abundances and ratios, the authors point out the relatively low Th/U of S-types to high Th/U of I-types, as we document in this present study.

In Fig. 3i, we plot >3.6 Ga from both igneous and detrital source rocks from the literature. Using our proposed Ce/U vs. Th/U discrimination, the majority of early Earth zircon have I-type chemistry, mostly overlapping the mantle domain. Interestingly, a few data do spread to lower Ce/U ratios, with only a limited number ($n = 4$) falling to lower Th/U ratios. The statistical importance of these analyses is uncertain, but at face value they point to a pure S-type component. Overall, the data imply that I-type magmatism is the dominant supplier of early Earth zircon. This conclusion does not rule out shallow melting involving peridotite (Borisova et al., 2022), melting in the deep crust (Burnham and Berry, 2017), or upper crustal tonalite differentiation (Laurent et al., 2022). It is noteworthy, however, that oxygen isotopes elevated above the mantle range imply the involvement of near-surface weathered material in early Earth zircon, though likely mixed in low proportions with an I-type in most cases.

6. Temporal S-type distribution

Using P contents, as well as the P vs REE+Y correlation, Zhu et al. (2020) calculated the distribution of S-type zircon that are present in a global detrital zircon dataset. Their results showed an increasing proportion of S-type zircon since 3 Ga, with a peak around 0.4 Ga correlating to granites formed through melting of widespread Gondwana sediments (see Fig. 6). They noted that although S-type abundance largely increases during periods of supercontinent assembly, the ca. 1 Ga Rodinia supercontinent had a muted increase relative to Columbia (2.0–1.6 Ga) and Gondwana (0.6 Ga). They suggested that this was a result of the plate margins involved in Rodinia assembly "were dominantly Andean in style, and produced neither the high mountains associated with continent-continent collisions, nor the stable platforms required for the accumulation of giant turbidite fans, both of which are essential for the formation of voluminous S-type granite suites".

We use the same approach to readdress the S-type distribution through time, combining a much larger detrital dataset (n = ~45,500 compared to ~7000; Roberts et al., 2024), and our proposed S-type discrimination tool. To discriminate 'Pure S-types', we use a cut-off at Ce/U = <0.01 (equivalent to log10[Ce/U] = <−2). We note that application of this cut-off alone will not discriminate 'metamorphic' zircon from those sourced from metapelitic melts. This caveat demonstrates the grey area between igneous and metamorphic processes, since partial melting during metamorphism ultimately leads to collection of melts into voluminous granitic bodies that can clearly be defined as an igneous feature. As such, our distribution of S-type anatectic melts likely also comprises some proportion from metamorphic rocks. This does not negate our objective however, as it still allows us to examine where and when sediment-melting was occurring, and whether the zircon are sourced from metapelites themselves, or voluminous granites, is irrelevant.

Our results have a clear distinction from those of Zhu et al. (2020), who used a discrimination based on P content that has shown to be unreliable (see above). Beyond ~3 Ga, the data are limited in number, but overall there is a similar increase from the late Archean through to the Phanerozoic. Our larger dataset reveals less marked drops during supercontinent tenure/break-up, suggesting that S-types may be formed more continuously through time than implied by Zhu et al. (2020). Peaks at 1.8 Ga, 1.0 Ga and 0.6 Ga broadly correlate with peaks in orogenesis as revealed by the metamorphic record (Brown and Johnson, 2018). In contrast to the result of Zhu et al. (2020), we find that the period of Rodinia amalgamation exhibits a high proportion of S-types; this observation suggests that orogenesis during this time was not necessarily any different to the preceding (Columbia) or subsequent (Gondwana) supercontinents. We argue that the most notable feature of our dataset, is a clear drop in S-type abundance during the ~1.7 – 1.2 Ga period. This period broadly correlates to the tenure and partial break-up of the Columbia supercontinent, which features a notable lack of collisional orogenesis and a dominance of accretionary orogenesis along the supercontinent margin (Roberts et al., 2022). The drop in S-type abundance can be explained by decreased sites of continental collision. Zhu

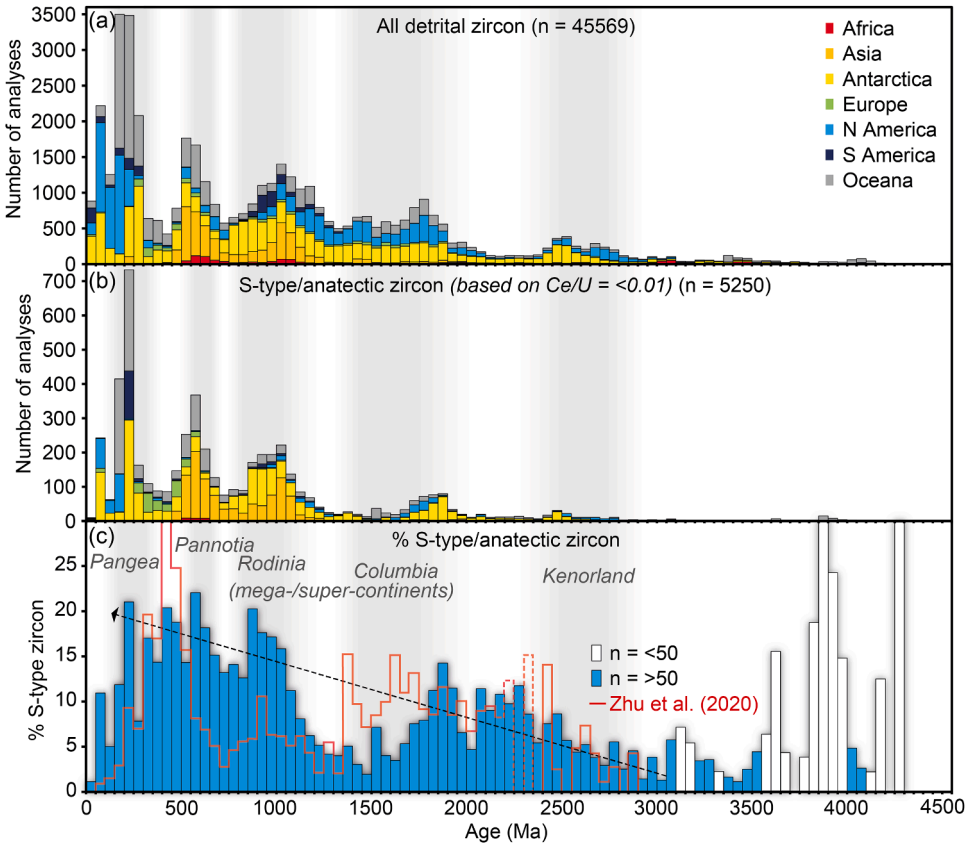

Fig. 6. (a) Histogram of filtered detrital zircon database divided by continent; (b) Histogram of S-type/anatectic zircon, based on a cut-off at Ce/U = <0.01, divided by continent; (c) Percentage of S-type zircon compared to total detrital zircon. Bin widths are 50 Myrs. Data with $n = < 50$ per bin are unfilled. The red line shows the % S-type zircon from Zhu et al. (2020). The black dashed line shows the broad increase in S-type abundance from ~3 Ga to the Phanerozoic. Shaded vertical bands show the estimated tenure of the supercontinents.

et al. (2020) argue that high mountains leading to deposition of widespread voluminous turbidites is a prerequisite for S-type formation. This process is responsible for formation of the Lachlan Fold Belt S-types, and any belt of voluminous S-type granite clearly require burial and melting of sediments; however, whether the presence or absence of S-types can be used to infer the scale and height of mountain belts is conjectural.

As noted in the Paleoarchean record in Fig. 3i, S-type-derived zircon proportion is low on Early Earth, and although the statistics are hampered by low abundance of data, it appears that ca. 2.5 Ga is the first rise to a significant component (>>5 %). This broadly coincides with some estimates for the widespread emergence of continents above sea-level (Flament et al., 2008), increasing granite diversity across the continents implying modern plate tectonic cycles (Laurent et al., 2014), and increasing reworking of sediments into magmas as documented by zircon $\delta^{18}O$ (Spencer et al., 2014). As such, our S-type distribution broadly agrees with a late Archean increase in sedimentary material available for reworking, and the amount of reworking recorded in the magmas. One caveat to this that provides an avenue for future research, is whether secular changes in sedimentary compositions (e.g. Taylor and McLennan, 1985) have a direct influence on zircon compositions that involve sedimentary protoliths.

7. Implications for Th/U-based zircon discrimination

Th/U ratios are commonly used to discriminate igneous from metamorphic zircon, although it is well known that zircon from high temperature metamorphic rocks overlap the igneous field (Harley et al., 2007; Rubatto, 2017; Yakymchuk et al., 2018). In detrital compilations, Th/U is often used as a cut-off to remove the inclusion of metamorphic zircon. However, our study demonstrates that some S-type granites, if formed through melting of metapelitic rocks, will have Th/U ratios overlapping the metamorphic field. Although such S-type magmas are anatectic in origin, they can clearly be categorized as an igneous rock unit. As such, removing data with Th/U < 0.1 from detrital datasets will potentially bias the results by removing S-type/anatectic granites. Th/U is also used in the interpretation of complex U-Pb datasets to discriminate those zircon domains resulting from metamorphic and magmatic processes; however, it may be that low Th/U merely relate to crystallisation of zircon in an anatectic environment, rather than relating to later post-crystallisation metamorphic resetting. Thus, our results suggest greater caution be used when using Th/U ratios.

8. Conclusion

We demonstrate that P contents in zircon are a poor discriminator of I- vs S-type granites, and that a range of magma compositions can exhibit P vs. REE+Y relationships with variable ratios of enrichment; these facts likely reflect the complex effects of melt chemistry on accessory mineral saturation, and imply the existence of multiple REE substitution mechanisms. We propose Ce/U vs Th/U as a tool to aid discrimination of granite types, with mantle-derived (I-type) zircon clearly being differentiated from metapelite-derived anatectic zircon (pure S-types). A limitation to these ratios is the overlap with metamorphic zircon. We emphasise the role of monazite in depleting Th and LREE in S-type melts. Strongly reducing conditions (low ΔFMQ) based on Ce-based oxybarometry for S-type and metapelitic zircon, suggests that the role of mineral co-crystallisation on Ce/U ratios (and therefore fO_2 calculations) may be more significant than previously considered, and that further investigation into the applicability of this proxy across a wider range of igneous suites is warranted. We highlight how Th/U ratios of S-

type granites can fall within the commonly applied metamorphic classification of < 0.1. A compilation of > 3.6 Ga zircon suggests that early Earth magmas that source these zircon may comprise a mixture of predominantly I-type and subordinately S-type magmas. Applying our Ce/U-based discrimination of S-type granites to a compilation of global detrital zircon, we show that: 1) S-type abundance increases in the late Archean; 2) in contrast to previous suggestions, S-type abundance is similar during Rodinia formation to other supercontinents; and 3) the 1.7–1.2 Ga period exhibits a marked drop in S-type abundance, compatible with a lack of continental collisions during this time.

Funding

NR and ST are partly supported by funding from the UK Natural Environment Research Council (NE/S011587/1). ST was supported by NERC Highlight Topic award "FAMOS" (From arc magmas to ores) NE/P01724X/1.

CRediT authorship contribution statement

Nick M W Roberts: Writing – original draft, Visualization, Investigation, Formal analysis, Data curation, Conceptualization. **Chris Yakymchuk:** Writing – review & editing, Visualization, Formal analysis. **Christopher J Spencer:** Writing – review & editing. **C. Brenhin Keller:** Writing – review & editing. **Simon R Tapster:** Writing – review & editing.

Declaration of competing interest

The authors declare that they have no known competing financial interests or personal relationships that could have appeared to influence the work reported in this paper.

Data availability

All new and published data used to create plots are provided at: https://figshare.com/s/1bc0e3c9daa3b8783000

Acknowledgements

The authors thank Rosemary Hickey-Vargas for efficient editorial handling, and the reviewers Olivier Bachmann and Elizabeth Bell for their constructive comments. The authors thanks those who shared samples for this study. NR and ST publish with the permission of the Director of the British Geological Survey, and are partly supported by funding from the UK Natural Environment Research Council (NE/S011587/1). ST was supported by NERC Highlight Topic award "FAMOS" (From arc magmas to ores) NE/P01724X/1.

Supplementary materials

Supplementary material associated with this article can be found, in the online version, at doi:10.1016/j.epsl.2024.118638.

References

Angelo, T.V., Spencer, C.J., Cavosie, A.J., Thomas, R., Li, H.Y., 2023. Petrogenesis of mantle-hosted granitoids from the samail ophiolite. J. Petrol. 64 (5), egad021.
Belousova, E.A., Griffin, W.L., O'Reilly, S.Y., Fisher, N.L., 2002. Igneous zircon: trace element composition as an indicator of source rock type. Contrib. Mineral. petrol. 143, 602–622.
Borisova, A.Y., Nédélec, A., Zagrtdenov, N.R., Toplis, M.J., Bohrson, W.A., Safonov, O.G., Bindeman, I.N., Melnik, O.E., Pokrovski, G.S., Ceuleneer, G., Jochum, K.P., 2022. Hadean zircon formed due to hydrated ultramafic protocrust melting. Geology 50 (3), 300–304.
Breiter, K., Lamarão, C.N., Borges, R.M.K., Dall'Agnol, R., 2014. Chemical characteristics of zircon from A-type granites and comparison to zircon of S-type granites. Lithos 192, 208–225.
Brown, M., Johnson, T., 2018. Secular change in metamorphism and the onset of global plate tectonics. Am. Mineral. 103 (2), 181–196.
Brudner, A., Jiang, H., Chu, X., Tang, M., 2022. Crustal thickness of the Grenville orogen: a Mesoproterozoic Tibet? Geology 50 (4), 402–406.
Bucholz, C.E., Stolper, E.M., Eiler, J.M., Breaks, F.W., 2018. A comparison of oxygen fugacities of strongly peraluminous granites across the Archean–Proterozoic boundary. J. Petrol. 59, 2123–2156.
Bucholz, C.E., 2022. Coevolution of sedimentary and strongly peraluminous granite phosphorus records. Earth Planet. Sci. Lett. 596, 117795.
Bucholz, C.E., Liebmann, J., Spencer, C.J., 2022. Secular variability in zircon phosphorus concentrations prevents simple petrogenetic classification. Geochem. Perspect. Lett. 24, 12–16.
Burnham, A.D., Berry, A.J., 2012. An experimental study of trace element partitioning between zircon and melt as a function of oxygen fugacity. Geochim. Cosmochim. Acta 95, 196–212.
Burnham, A.D., Berry, A.J., 2017. Formation of Hadean granites by melting of igneous crust. Nat. Geosci. 10 (6), 457–461.
Carley, T.L., Miller, C.F., Wooden, J.L., Padilla, A.J., Schmitt, A.K., Economos, R.C., Bindeman, I.N., Jordan, B.T., 2014. Iceland is not a magmatic analog for the Hadean: evidence from the zircon record. Earth Planet. Sci. Lett. 405, 85–97.
Castiñeiras, P., García, F.D., Barreiro, J.G., 2010. REE-assisted U–Pb zircon age (SHRIMP) of an anatectic granodiorite: constraints on the evolution of the A Silva granodiorite, Iberian allochthonous complexes. Lithos 116 (1–2), 153–166.
Castineiras, P., Navidad, M., Casas, J.M., Liesa, M., Carreras, J., 2011. Petrogenesis of Ordovician magmatism in the Pyrenees (Albera and Canigó Massifs) determined on the basis of zircon minor and trace element composition. J. Geol. 119 (5), 521–534.
Chappell, B.W., White, A.J.R., 1974. Two contrasting granite types. Pac. Geol. 8, 173–174.
Chappell, B.W., White, A.J.R., 1992. I-and S-type granites in the Lachlan fold belt. Earth Environ. Sci. Trans. R. Soc. Edinb. 83 (1–2), 1–26.
Chen, R.X., Zheng, Y.F., 2017. Metamorphic zirconology of continental subduction zones. J. Asian Earth. Sci. 145, 149–176.
Chen, Z., 2023. Europium anomalies in detrital zircons reveal the crustal thickness evolution of South China in early neoproterozoic. Acta Geochimica. 1–8.
Clemens, J.D., Stevens, G., Farina, F., 2011. The enigmatic sources of I-type granites: the peritectic connexion. Lithos 126 (3–4), 174–181.
Drabon, N., Byerly, B.L., Byerly, G.R., Wooden, J.L., Wiedenbeck, M., Valley, J.W., Kitajima, K., Bauer, A.M., Lowe, D.R., 2022. Destabilization of long-lived Hadean Protocrust and the onset of pervasive hydrous melting at 3.8 Ga. AGU Adv. 3 (2), e2021AV000520.
Flament, N., Coltice, N., Rey, P.F., 2008. A case for late-Archaean continental emergence from thermal evolution models and hypsometry. Earth Planet. Sci. Lett. 275 (3–4), 326–336.
Foden, J., Sossi, P.A., Wawryk, C.M., 2015. Fe isotopes and the contrasting petrogenesis of A-, I-and S-type granite. Lithos 212, 32–44.
Frost, B.R., Barnes, C.G., Collins, W.J., Arculus, R.J., Ellis, D.J., Frost, C.D., 2001. A geochemical classification for granitic rocks. J. Petrol. 42 (11), 2033–2048.
Grimes, C.B., John, B.E., Kelemen, P.B., Mazdab, F.K., Wooden, J.L., Cheadle, M.J., Hanghøj, K., Schwartz, J.J., 2007. Trace element chemistry of zircons from oceanic crust: a method for distinguishing detrital zircon provenance. Geology 35 (7), 643–646.
Grimes, C.B., Wooden, J.L., Cheadle, M.J., John, B.E., 2015. Fingerprinting" tectono-magmatic provenance using trace elements in igneous zircon. Contrib. Mineral. Petrol. 170, 1–26.
Harlaux, M., Kouzmanov, K., Gialli, S., Clark, A.H., Laurent, O., Corthay, G., Flores, E.P., Dini, A., Chauvet, A., Ulianov, A., Chiaradia, M., 2021. The upper Oligocene San Rafael intrusive complex (eastern Cordillera, southeast Peru), host of the largest-known high-grade tin deposit. Lithos 400, 106409.
Harley, S.L., Kelly, N.M., Möller, A., 2007. Zircon behaviour and the thermal histories of mountain chains. Elements 3 (1), 25–30.
Harrison, T.M., 2009. The Hadean crust: evidence from>4 Ga zircons. Annu. Rev. Earth Planet. Sci. 37, 479–505.
Harrison, T.M., 2020. Hadean jack hills zircon geochemistry. Hadean Earth. Springer, Cham, pp. 143–178.
Healy, B., Collins, W.J., Richards, S.W., 2004. A hybrid origin for Lachlan S-type granites: the Murrumbidgee batholith example. Lithos 78 (1–2), 197–216.
Hopkinson, T.N., Harris, N.B., Warren, C.J., Spencer, C.J., Roberts, N.M., Horstwood, M. S., Parrish, R.R., 2017. The identification and significance of pure sediment-derived granites. Earth Planet. Sci. Lett. 467, 57–63.
Hoskin, P.W., Ireland, T.R., 2000. Rare earth element chemistry of zircon and its use as a provenance indicator. Geology 28 (7), 627–630.
Hoskin, P.W., Schaltegger, U., 2003. The composition of zircon and igneous and metamorphic petrogenesis. Rev. Mineral. Geochem. 53 (1), 27–62.
Keay, S., Collins, W.J., McCulloch, M.T., 1997. A three-component Sr-Nd isotopic mixing model for granitoid genesis, Lachlan fold belt, eastern Australia. Geology 25 (4), 307–310.
Laurent, O., Martin, H., Moyen, J.F., Doucelance, R., 2014. The diversity and evolution of late-Archean granitoids: Evidence for the onset of "modern-style" plate tectonics between 3.0 and 2.5 Ga. Lithos 205, 208–235.
Laurent, O., Moyen, J.F., Wotzlaw, J.F., Björnsen, J., Bachmann, O., 2022. Early Earth zircons formed in residual granitic melts produced by tonalite differentiation. Geology 50 (4), 437–441.

Liu, H., McKenzie, N.R., Colleps, C.L., Chen, W., Ying, Y., Stockli, L., Sardsud, A., Stockli, D.F., 2022a. Zircon isotope–trace element compositions track Paleozoic–Mesozoic slab dynamics and terrane accretion in Southeast Asia. Earth Planet. Sci. Lett. 578, 117298.
Liu, Z., Zhang, G., Xiong, L., Chang, F., Liu, S., 2022b. Evolution of the continental crust in the northern Tibetan Plateau: constraints from geochronology and Hf isotopes of detrital zircons. Front. Earth. Sci. (Lausanne) 669.
Loucks, R.R., Fiorentini, M.L., Henríquez, G.J., 2020. New magmatic oxybarometer using trace elements in zircon. J. Petrol. 61 (3), egaa034.
Loucks, R.R., Fiorentini, M.L., Rohrlach, B.D., 2018. Divergent T–fO_2 paths during crystallisation of H_2O-rich and H_2O-poor magmas as recorded by Ce and U in zircon, with implications for TitaniQ and TitaniZ geothermometry. Contrib. Mineral. Petrol. 173, 1–21.
Marsh, J.H., Stockli, D.F., 2015. Zircon U–Pb and trace element zoning characteristics in an anatectic granulite domain: insights from LASS-ICP-MS depth profiling. Lithos 239, 170–185.
Martin, L.A., Duchêne, S., Deloule, E., Vanderhaeghe, O., 2008. Mobility of trace elements and oxygen in zircon during metamorphism: consequences for geochemical tracing. Earth Planet. Sci. Lett. 267 (1–2), 161–174.
Mojzsis, S.J., Harrison, T.M., Pidgeon, R.T., 2001. Oxygen-isotope evidence from ancient zircons for liquid water at the Earth's surface 4,300Myr ago. Nature 409 (6817), 178–181.
Reimink, J.R., Davies, J.H., Bauer, A.M., Chacko, T., 2020. A comparison between zircons from the Acasta Gneiss Complex and the Jack Hills region. Earth Planet. Sci. Lett. 531, 115975.
Roberts, N.M.W., Spencer, C.J., Puetz, S., Keller, C.B. and Tapster, S.R., 2024. Regional trends and petrologic factors inhibit global interpretations of detrital zircon trace element compositions. EarthArXiv [Preprint] Available from: https://doi.org/10.31223/X55D7R.
Roberts, N.M.W., Salminen, J., Johansson, Å., Mitchell, R.N., Palin, R.M., Condie, K.C., Spencer, C.J., 2022. On the enigmatic mid-Proterozoic: single-lid versus plate tectonics. Earth Planet. Sci. Lett. 594, 117749.
Roberts, N.M.W., Spencer, C.J., 2015. The zircon archive of continent formation through time. Geol. Soc. Lond. Spec. Publ. 389 (1), 197–225.
Rollinson, H., 2015. Slab and sediment melting during subduction initiation: granitoid dykes from the mantle section of the Oman ophiolite. Contrib. Mineral. Petrol. 170, 1–20.
Rubatto, D., 2002. Zircon trace element geochemistry: partitioning with garnet and the link between U–Pb ages and metamorphism. Chem. Geol. 184 (1–2), 123–138.
Rubatto, D., 2017. Zircon: the metamorphic mineral. Rev. Mineral. Geochem. 83 (1), 261–295.
Sawaki, Y., Asanuma, H., Sakata, S., Abe, M., Ohno, T., 2022a. Trace-element composition of zircon in Kofu and Tanzawa granitoids, Japan: quantitative indicator of sediment incorporated in parent magma. Island Arc. 31 (1), e12455.
Sawaki, Y., Asanuma, H., Sakata, S., Abe, M., Ohno, T., 2022b. Zircon trace-element compositions in Miocene granitoids in Japan: discrimination diagrams for zircons in M-, I-, S-, and A-type granites. Island Arc. 31 (1), e12466.
Spencer, C.J., Cawood, P.A., Hawkesworth, C.J., Raub, T.D., Prave, A.R., Roberts, N.M., 2014. Proterozoic onset of crustal reworking and collisional tectonics: reappraisal of the zircon oxygen isotope record. Geology 42 (5), 451–454.
Spencer, C.J., Cavosie, A.J., Raub, T.D., Rollinson, H., Jeon, H., Searle, M.P., Miller, J.A., McDonald, B.J., Evans, N.J., 2017. Evidence for melting mud in Earth's mantle from extreme oxygen isotope signatures in zircon. Geology 45 (11), 975–978.
Stimac, J.A., Clark, A.H., Chen, Y., Garcia, S., 1995. Enclaves and their bearing on the origin of the Cornubian batholith, southwest England. Mineral. Mag. 59 (395), 273–296.
Tang, M., Chu, X., Hao, J., Shen, B., 2021. Orogenic quiescence in Earth's middle age. Science 371 (6530), 728–731.
Taylor, S.R. and McLennan, S.M., 1985. The continental crust: its composition and evolution.
Wang, Q., Zhu, D.C., Zhao, Z.D., Guan, Q., Zhang, X.Q., Sui, Q.L., Hu, Z.C., Mo, X.X., 2012. Magmatic zircons from I-, S-and A-type granitoids in Tibet: trace element characteristics and their application to detrital zircon provenance study. J. Asian Earth. Sci. 53, 59–66.
Wooden, J.L., Mazdab, F.K., Barth, A.P., Miller, C.F., Lowery, L.E., 2006. Temperatures (TI) and compositional characteristics of zircon: early observations using high mass resolution on the USGS-Stanford SHRIMP-RG. Geochim. Cosmochim. Acta 70 (18), A707.
Yakymchuk, C., Holder, R.M., Kendrick, J., Moyen, J.F., 2023. Europium anomalies in zircon: a signal of crustal depth? Earth Planet. Sci. Lett. 622, 118405.
Yakymchuk, C., Kirkland, C.L., Clark, C., 2018. Th/U ratios in metamorphic zircon. J. Metamorph. Geol. 36 (6), 715–737.
Zhong, S., Li, S., Liu, Y., Cawood, P.A., Seltmann, R., 2023a. I-type and S-type granites in the Earth's earliest continental crust. Commun. Earth. Environ. 4 (1), 61.
Zhong, S.H., Liu, Y., Li, S.Z., Bindeman, I.N., Cawood, P.A., Seltmann, R., Niu, J.H., Guo, G.H., Liu, J.Q., 2023b. A machine learning method for distinguishing detrital zircon provenance. Contrib. Mineral. Petrol. 178 (6), 35.
Zhu, Z., Campbell, I.H., Allen, C.M., Burnham, A.D., 2020. S-type granites: their origin and distribution through time as determined from detrital zircons. Earth Planet. Sci. Lett. 536, 116140.